Investigation of Resonance Based Propagation Loss Modeling for THz Chip-to-Chip Wireless Communications

Jinbang Fu, Prateek Juyal, Baki Berkay Yilmaz, and Alenka Zajić *Senior Member, IEEE*
Georgia Institute of Technology, Atlanta, GA 30332 USA

***Abstract*—This paper proposes a path loss model for THz chip-to-chip wireless communication in desktop size metal enclosures with respect to transceivers positions. This path loss model accounts for the attenuation due to the signal spreading, resonant modes inside the cavity, and the radiation pattern of the antenna. Measurements were performed in LoS and 2-D and 3-D misalignment propagation scenarios. The model prediction shows a good agreement with measured results, which proves the validness of the model.**

***Index Terms*—path loss model, THz communications, propagation, measurements.**

I. Introduction

With the development of cellular networks (3G, 4G, and upcoming 5G) and wireless local area networks (WLAN), wireless communication is approaching promised high speed and low latency communications. The ever-growing capabilities of wireless communication systems which make more data rate available to users fosters the growth of many new applications such as remote surgery, autonomous driving, smart cities, and wireless short range communications. Especially for the short range communication between devices in a desktop, wireless communication is considered a future solution that can alleviate the cable management problem and reduce the complexity of system design and maintenance. However, current wireless communication systems cannot match the required data rate. For example, existing systems use up to 600 Gb/s with InniBand HDR 12 link [1], while current wireless communication systems can only achieve 10 Gb/s at 5 GHz frequency band with the new IEEE802.11ax standard, MIMO-OFDM modulation, and complicated coding [2] schemes. Terahertz (THz) frequency band is one of the most promising ways to overcome gap between wired and wireless communications in computer systems [3] and provide additional communication links between processor and memory or between blades in a data center [4].

To develop THz wireless communication schemes for chip-to-chip communications, the first step is to understand the propagation mechanisms inside a metal cavity. At THz frequencies, there has been a large number of measurement campaigns that characterize indoor propagation environment including line-of-sight (LoS), non-line-of-sight (NLoS) propagation, angles of departure and arrival, shadowing effects, and reflection and diffraction from various materials [4]–[10]. Measurements have also been conducted to characterize waveguide-like structures with different dimensions at 60 and 300 GHz for intra-device communications [11]. Furthermore, on-board THz wireless communication measurements have been conducted by considering different possible scenarios, i.e., LoS, reflected-non-line-of-sight (RNLoS), NLoS, and obstructed-line-of-sight (OLoS) [9]. Finally, the channel measurements at 300 GHz inside a desktop size metal enclosure have been performed [7], [8].

Based on propagation mechanisms, several path loss models have been proposed and compared for THz wireless channels [8], [12]–[15]. Path loss for traveling EM wave in THz band has been modeled as the summation of the spreading loss and the molecular absorption attenuation in [12], [13]. A path loss model which accounts the propagation loss of THz radiation through vegetation has been proposed in [14] by considering the attenuation and scattering effect of the air and leaves. For the wireless channels in indoor environment, the performances of different large-scale path loss models at 30 GHz, 140 GHz, and 300 GHz have been compared in [15]. Different from the EM wave propagation in free space, THz propagation in metal enclosures experiences both traveling and resonant waves [7], [8]. This yields to larger number of multiple reflections as well as larger multipath spread [8]. Also, due to the resonant nature of the fields, the received power can vary with transceivers positions. Based on these findings, an initial path loss model in an empty desktop size metal enclosure has been proposed as a function of transceiver's height in [8].

As the continuation of work [8], this paper presents the complete path loss model for THz chip-to-chip communication in metal enclosures. Based on the cavity environment and the characteristics of the channel inside the metal cavity observed through measurements [7], we propose the model that is the combination of the signal spreading loss, power fluctuation due to resonant modes, and the effect of antenna radiation pattern. Measurements were performed by moving the transceivers in only vertical direction (2-D case) and in both vertical and horizontal direction (3-D case) with the consideration of LoS propagation and the misalignment between the transmitter (Tx)

This work has been supported, in part, by NSF grant 1651273. The views and findings in this paper are those of the authors and do not necessarily reflect the views of NSF.

and receiver (Rx). The results show a good agreement between the simulated and measured statistics.

The remainder of the paper is organized as follows. Section II presents the path loss model that includes channel properties inside a metal cavity. Section III verifies the path loss model by comparing the modeled path loss with measured results for different scenarios. Section IV provides concluding remarks.

II. Path Loss Model

This section introduces a new path loss model to approximate the propagation loss inside a desktop size metal cavity. Unlike the wireless communication in free space, THz chip-to-chip wireless communication is much more sophisticated due to the cavity effect present in the metal enclosure. Hence, for the THz wireless channel inside a metal cavity, it is not sufficient to model the propagation loss with Friis equation only. From channel measurements, it was found that both traveling wave and resonant modes exist inside the metal cavity [7], [8]. Therefore, another term is required to depict the effect of resonant modes. Additionally, to compensate for a high path loss of THz channel, both Tx and Rx are always equipped with high gain antennas [16]. Hence, the radiation pattern of the antennas should be considered. In addition, molecular absorption can be significant at THz frequencies. However, measured values shown in [17] imply that it is negligible at the distance less than 1 m. For on-board intra-chip communication, this loss can be neglected.

Therefore, for THz wireless channel in a metal enclosure, the theoretical path loss $(PL)_{dB}$ can be expressed as

$$\begin{aligned}(PL)_{dB} =&\overline{(PL)^t_{dB}} + 10\log_{10}(|E|^2)^{-1} \\ &+ 10\log_{10}([g(\alpha_t)g(\alpha_r)]^2)^{-1} + X_\sigma, \end{aligned} \quad (1)$$

where $\overline{(PL)^t_{dB}}$ is the mean path loss of traveling wave. It can be calculated by averaging Friis formula over the available bandwidth of the channel as

$$\overline{(PL)^t_{dB}} = \frac{1}{BW}\int_{BW}\frac{4\pi d^{\frac{\gamma}{2}} f}{c_0} df, \quad (2)$$

where BW, d, γ, and c_0 represent bandwidth of the channel, signal traveled distance, path loss exponent, and the speed of light, respectively.

The term $10\log_{10}(|E|^2)^{-1}$ represents the received power variation due to the resonant modes inside the metal cavity. For Tx and Rx equipped with directional horn antennas, only transverse electric (TE) modes are considered. Hence, $|E|^2$ can be written as

$$\begin{aligned}|E|^2 &= |E_x|^2 + |E_y|^2 \\ &= \left|\sum_{m=0}^{M}\sum_{n=0}^{N}\sum_{p=0}^{P} Ex_{mnp}\right|^2 + \left|\sum_{m=0}^{M}\sum_{n=0}^{N}\sum_{p=0}^{P} Ey_{mnp}\right|^2, \end{aligned} \quad (3)$$

where M, N, and P define the number of dominant TE modes inside the cavity. The expressions of Ex_{mnp} and Ey_{mnp} are given in [18] as

$$Ex_{mnp} = -\frac{j\omega_{mnp}\mu k_x H_0}{k^2_{mnp} - k^2_z}\cos(\frac{m\pi x}{a})\sin(\frac{n\pi y}{b})\sin(\frac{p\pi z}{c}), \quad (4)$$

$$Ey_{mnp} = \frac{j\omega_{mnp}\mu k_y H_0}{k^2_{mnp} - k^2_z}\sin(\frac{m\pi x}{a})\cos(\frac{n\pi y}{b})\sin(\frac{p\pi z}{c}), \quad (5)$$

where H_0 is an arbitrary constant with units of A/m and m, n, and p are integers. Eigenvalue k_{mnp} satisfies

$$k^2_{mnp} = k^2_x + k^2_y + k^2_z = (\frac{m\pi}{a})^2 + (\frac{n\pi}{b})^2 + (\frac{p\pi}{c})^2, \quad (6)$$

where a, b, and c represent the height, width, and length of the cavity as shown in Fig. 1. The resonant frequencies can be determined as

$$f_{mnp} = \frac{1}{2\sqrt{\mu\epsilon}}\sqrt{\left(\frac{m}{a}\right)^2 + \left(\frac{n}{b}\right)^2 + \left(\frac{p}{c}\right)^2}, \quad (7)$$

where ϵ and μ are the permittivity and permeability.

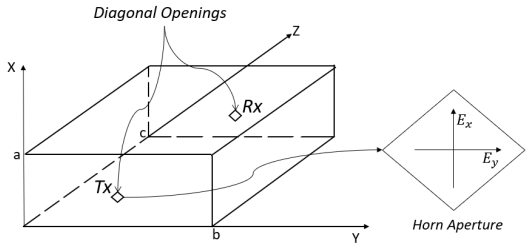

Fig. 1. Rectangular metal cavity with diagonal openings

The term $10\log_{10}([g(\alpha_t)g(\alpha_r)]^2)^{-1}$ describes the loss due to the misalignment between the Tx and Rx. Parameters α_t and α_r represent the angle of departure (AoD) and the angle of arrival (AoA), respectively. The parameter $g(\alpha)$ is the radiation pattern of the equipped antenna. For diagonal horn antenna which has been used for our measurements, $g(\alpha)$ can be expressed as [19]

$$g(\alpha) = \begin{cases} X + Y\cos(Z\alpha) & -\theta \le \alpha \le \theta \\ c & otherwise \end{cases}, \quad (8)$$

where θ is half beamwidth of the diagonal horn antenna and c represents a small constant.

X_σ is the error between the predicted and actual path loss, which can be modeled as a zero-mean Gaussian random variable with standard deviation σ.

III. Measurements And Model Verification

To verify the proposed path loss model, we have performed measurements and compared results with simulations in this section. For the model verification, both two dimensional (2-D) and three dimensional (3-D) cases were considered. For the 2-D case, the relationship between path loss and heights of transceivers was explored with measurements and captured

by our model. The geometry of the metal cavity is shown in Fig. 1. Denoting the phase centers' coordinates of Tx and Rx as (x_t, y_t, z_t) and (x_r, y_r, z_r), respectively, only x_t and x_r are in variation for this case. For the 3-D case, only z_t and z_r are fixed (the length of the cavity is fixed). Path loss was measured and captured by the model with the variation of x_t, y_t, x_r, and y_r.

A. 2-D

For the 2-D configuration, since the movement of transceivers is only in x direction, equations (4) and (5) can be rewritten as

$$Ex_m = A_m \cos(\frac{m\pi x}{a}), \tag{9}$$

$$Ey_m = B_m \sin(\frac{m\pi x}{a}), \tag{10}$$

where A_m and B_m are coefficients for the m_{th} TE mode. Also, equation (3) can be simplified to

$$|E|^2 = |E_x|^2 + |E_y|^2 = \left|\sum_{m=1}^{M} Ex_m\right|^2 + \left|\sum_{m=1}^{M} Ey_m\right|^2. \tag{11}$$

To verify the model, a set of measurements was performed inside a desktop size, 30.5 cm × 30.5 cm × 9.6 cm, metal enclosure with two different scenarios being considered.

The first scenario is the LoS propagation inside the empty metal cavity. Measurements were performed by varying the heights of transceivers, h_t and h_r, simultaneously from 0 cm to 6.6 cm with the step size of 0.6 cm. Transceivers' heights, h_t and h_r, refer to the distances from the bottom edge of the equipped horn antennas to the ground of the metal cavity. The measurement setup is shown in Fig. 2a. Diagonal horn antennas were used with gain that varies between 22 dBi and 23 dBi with 3 dB beamwidths about 12°, i.e., $2\theta_t = 2\theta_r = 12°$. Please note that the distance between the phase center and bottom edge of the horn is 0.4575 cm, which means that $x_t = x_r = h_t/h_r + 0.4575$ cm. By cuve-fitting the EM simulated radiation pattern of the equipped antennas, the parameters of the radiation pattern $g(\alpha)$ are found to be $X = 0.54$, $Y = 0.45$, $Z = 11.15$, and $c = 0.01$. Measured data was collected at the frequency from 300 GHz to 312 GHz.

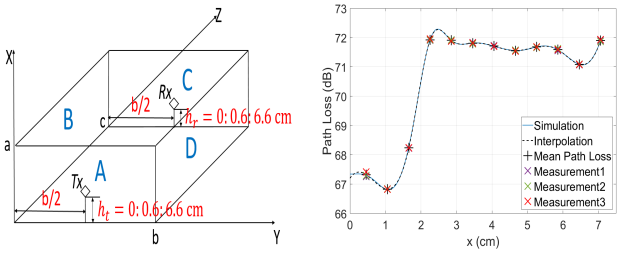

(a) (b)

Fig. 2. Exploration of LoS propagation in an empty metal cavity at 300 GHz for 2-D case: (a) Measurements setup, (b) Comparison of theoretical and measured path loss with respect to transceiver's height.

Figure 2b compares the measured and model predicted path loss. It can be observed that the path loss predicted by the model matches well with the measured results. It is found that the first eight TE modes ($M = 8$) dominate the channel. The coefficients, A_m and B_m for each mode were found by curve-fitting the interpolated measured mean path loss and shown in [8]. We did three measurements for each height of the transceivers and the difference between these three measured results, as shown in Fig. 2b, is very small. This is because the channel is stationary with fixed h_t and h_r, which means that there are no temporal or spatial variations in the channel which would lead to signicant change of the path loss. Although some variation can still be observed, this may be due to the variation of the resonant modes inside the cavity. Via least square linear fitting, parameters of the model, γ and σ, are estimated to be 1.9874 and 0.0239dB.

The second scenario is the LoS propagation with a misalignment of the Tx and Rx as shown in Fig. 3a. The measurement setup is similar as the first scenario with h_t being fixed at 2.4 cm and h_r being varied from 0 cm to 6.6 cm with the step size of 0.6 cm. Measurements were performed 10 times at each height of the Rx and the results are shown in Fig. 3b. Similar to the first scenario, the variation between different measured path loss is small for any given h_r since there are no temporal and spacial changes in the channel. Based on the height difference between Tx and Rx, the values of d, AoD, and AoA can be calculated for different h_r. With known coefficients A_m, B_m for different dominate modes and the path loss exponent γ, path loss can be predicted from the model. Figure 3b compares the measured results and the model prediction. From the plot, a good agreement can be observed, which proves the validity of our proposed model. The parameter σ is estimated to be 0.5532 dB from the measurements.

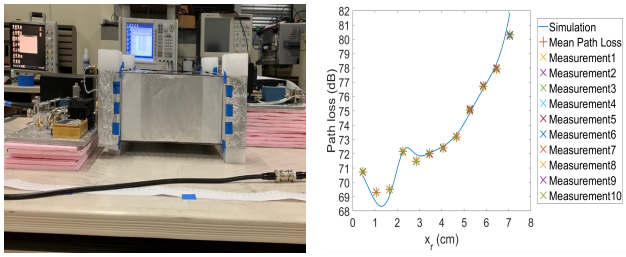

(a) (b)

Fig. 3. Exploration of LoS propagation in an empty metal cavity at 300 GHz with a misalignment between Tx and Rx for 2-D case: (a) Measurements setup, (b) Comparison of theoretical and measured path loss with respect to x_r.

B. 3-D

For the 3-D figuration, transceivers are moved along the x and y direction with fixed z_t and z_r as shown in Figs. 5a & 6a. For this scenario, Ex_{mnp} and Ey_{mnp} can be written as

$$Ex_{mn} = A_{mn} \cos(\frac{m\pi x}{a}) \sin(\frac{n\pi y}{b}), \tag{12}$$

$$Ey_{mn} = B_{mn} \sin(\frac{m\pi x}{a}) \cos(\frac{n\pi y}{b}), \tag{13}$$

where A_{mn} and B_{mn} are the coefficients for the mode TE_{mn}. Furthermore, equation (3) can also be simplified to

$$|E|^2 = |E_x|^2 + |E_y|^2 = \left|\sum_{m=0}^{M}\sum_{n=0}^{N} Ex_{mn}\right|^2 + \left|\sum_{m=0}^{M}\sum_{n=0}^{N} Ey_{mn}\right|^2. \quad (14)$$

For the exploration of the 3-D configuration, another metal cavity was fabricated with size of $30.5\ \text{cm} \times 30.5\ \text{cm} \times 10\ \text{cm}$, which approximates the size of a computer desktop casing. As shown in Fig. 4, two square aluminum plates are fixed by nylon board spacers at four corners to form the top and bottom wall of the cavity. The other four sides of the cavity are wrapped by aluminum foils and labeled as A, B, C, and D. Measurements were performed inside the metal cavity with two different scenarios being considered to verify the proposed model.

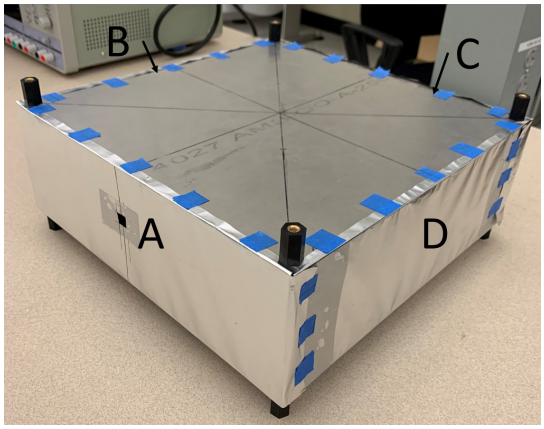

Fig. 4. New metal cavity

For the first scenario, the LoS propagation was explored. The metal cavity was put in between the Tx and Rx with two antennas aligned with each other. Diagonal openings with the horn size were drilled on the transceivers sides (side A and C) of the metal cavity. As shown in Fig. 5a, both Tx and Rx were moved in x direction with $d_x = 0.6075 : 0.6 : 5.4575$ cm and in y direction with $d_y = 0 : 4 : 12$ cm. Since z_t and z_r are fixed, the relative locations of transceivers' phase centers can be specified as $x_t = x_r = dx$, $y_t = y_r = dy + \frac{b}{2}$, $z_t = 0$ cm, and $z_r = 30.5$ cm, where b is the length of the metal cavity which is 30.5 cm. At each location, measurements were performed 10 times. Figure 5b compares the measured results and their mean value at each location, and the interpolation of mean path loss. As shown in the plot, variation of the path loss along the x direction is similar as the result of the 2-D case shown in Fig.2b. Compared with the 5 dB variation along the x direction, the changes of path loss along the y direction are less than 1 dB. This is because transceivers were put far from the side walls B and D of the cavity (the distance is greater then 3 cm) during the measurements, which means that the reflections on the side walls have little effect to the path loss. Additionally, the width of the cavity is 305 times of the wavelength, which means that the effect of resonant modes in y direction is small. Also, it can be observed that the variation of measured results is small at each location since the channel is stationary without strong temporal and spacial variation. From the measurements, the standard deviation of variation factor, σ, is determined to be 0.0176 dB.

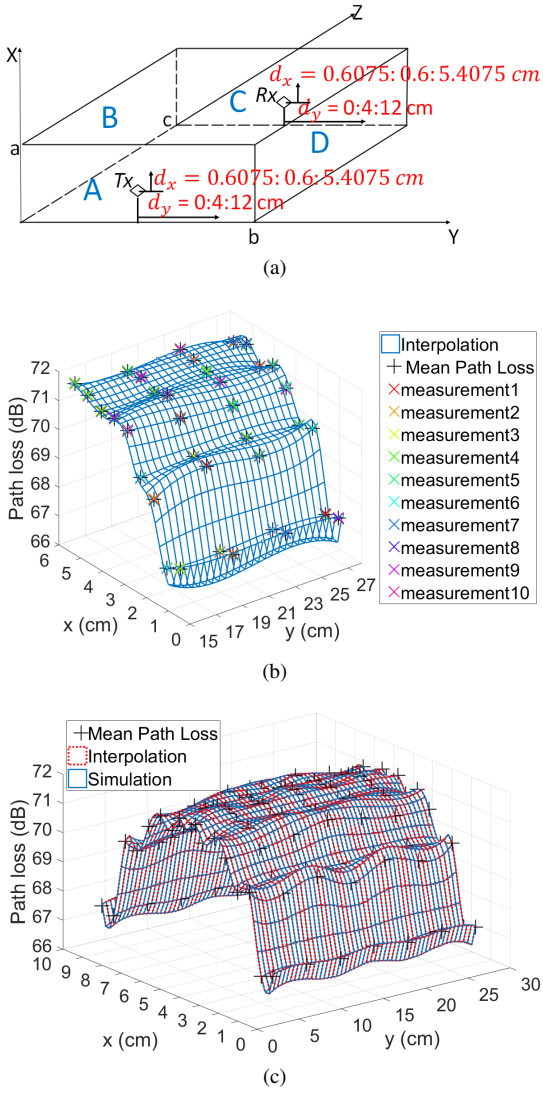

Fig. 5. Exploration of LoS propagation in an empty metal cavity at 300 GHz for 3-D case: (a) Measurements setup, (b) Measured results, (c) Comparison of theoretical and measured path loss with respect to x_t/x_r and y_t/y_r.

The path loss variation in the area where x_t/x_r varies from 0.6075 to 5.4075 cm and y_t/y_r varies from 15.25 to 27.25 cm was measured and shown in Fig. 5b. To model the path loss variation inside the metal cavity, more measured results in a larger area are required. Since the metal cavity is symmetric, we exploit it to reduce the number of measurements. By doing this, the change of path loss in the area where x_t/x_r varies from 0.6075 to 9.3725 cm and y_t/y_r varies from 3.25 to 27.25 cm can be estimated. By interpolating and curve-fitting, parameters M and N that define the dominant modes inside the cavity are determined to be 25 and 13, respectively. Also, the coefficients A_{mn} and B_{mn} are estimated for each mode. To minimize the least square error of the curve-fitting, the path

loss exponent γ is estimated to be 1.9995. Figure 5c compares model prediction with the mean value of measured results at each location after flipping and the interpolation. It can be observed from Fig. 5c that the model matches well with the measured results.

The second scenario, again, explores the LoS propagation with a misalignment between the Tx and Rx. In this scenario, as shown in Fig. 6a., measurements were performed with both Tx and Rx being moved vertically with x_t/x_r varying from 0.6075 to 5.4075 cm with the step size of 1.2 cm. Also at each height, Rx was moved in y direction with y_r varying from 15.25 to 18.25 cm with the step size of 1 cm. At each location, measurements were performed 10 times. Based on the difference between y_t and y_r at each location, path loss can be estimated with the known parameters A_{mn}, B_{mn}, and γ. Figure 6b compares the model prediction with measured results. As shown in the plot, since the channel is stationary, the difference between measured results at each location is small. Also, a good agreement between the measured and predicted path loss can be observed from the plot, which again confines the correctness of the model. Based on the measurements, the standard deviation of the shadowing factor, σ is estimated to be 0.2715 dB for this scenario.

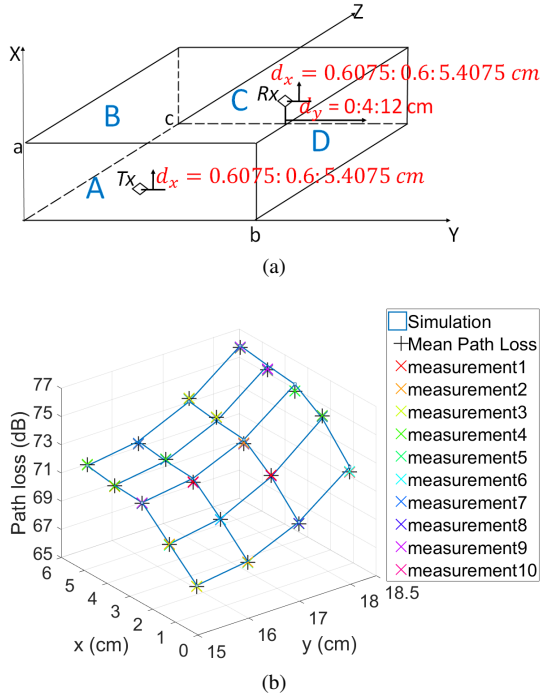

Fig. 6. LoS propagation in an empty metal cavity at 300 GHz with a misalignment between Tx and Rx: (a) Measurements setup, (b) Comparison of theoretical and measured path loss with respect to h_r.

IV. Conclusions

In this paper we present the path loss model for THz chip-to-chip wireless communication in desktop size metal enclosures with the consideration of both 2-D an 3-D Tx/Rx misalignment. This path loss model accounts for the attenuation due to the signal spreading, resonant modes inside the cavity, and the radiation pattern of the antenna, which makes it different from traditional path loss models. Measurements were performed for scenarios of LoS propagation and misalignment between transceivers to validate the model. A good agreement between the measured and simulated results was observed.

References

[1] InifiBand. (2018) Infiniband roadmap. [Online]. Available: https://www.infinibandta.org/infiniband-roadmap/

[2] P. C. Jain, "Recent trends in next generation terabit ethernet and gigabit wireless local area network," in *2016 International Conference on Signal Processing and Communication (ICSC)*, Dec 2016, pp. 106–110.

[3] T. Kürner, "THz communications: Challenges and applications beyond 100 gbit/s," in *2018 International Topical Meeting on Microwave Photonics (MWP)*, Oct 2018, pp. 1–4.

[4] C. Cheng and A. Zajić, "Characterization of 300 GHz wireless channels for rack-to-rack communications in data centers," in *2018 IEEE 29th Annual International Symposium on Personal, Indoor and Mobile Radio Communications (PIMRC)*, Sep. 2018, pp. 194–198.

[5] M. Jacob, S. Priebe, R. Dickhoff, T. Kleine-Ostmann, T. Schrader, and T. Kürner, "Diffraction in mm and sub-mm wave indoor propagation channels," *IEEE Transactions on Microwave Theory and Techniques*, vol. 60, no. 3, pp. 833–844, March 2012.

[6] A. Fricke, S. Rey, M. Achir, P. Le Bars, T. Kleine-Ostmann, and T. Kürner, "Reflection and transmission properties of plastic materials at THz frequencies," in *2013 38th International Conference on Infrared, Millimeter, and Terahertz Waves (IRMMW-THz)*, Sep. 2013, pp. 1–2.

[7] J. Fu, P. Juyal, and A. Zajić, "300 GHz channel characterization of chip-to-chip communication in metal enclosure," in *2019 13th European Conference on Antennas and Propagation (EuCAP)*, March 2019, pp. 1–5.

[8] ——, "THz channel characterization of chip-to-chip communication in desktop size metal enclosure," *IEEE Transactions on Antennas and Propagation*, pp. 1–1, 2019.

[9] S. Kim and A. Zajić, "Characterization of 300-GHz wireless channel on a computer motherboard," *IEEE Transactions on Antennas and Propagation*, vol. 64, no. 12, pp. 5411–5423, Dec 2016.

[10] S. Kim and A. G. Zaji, "Statistical characterization of 300-ghz propagation on a desktop," *IEEE Transactions on Vehicular Technology*, vol. 64, no. 8, pp. 3330–3338, Aug 2015.

[11] T. Kürner, A. Fricke, S. Rey, P. Le Bars, A. Mounir, and T. Kleine-Ostmann, "Measurements and modeling of basic propagation characteristics for intra-device communications at 60 GHz and 300 GHz," *Journal of Infrared, Millimeter, and Terahertz Waves*, vol. 36, no. 2, pp. 144–158, 2015.

[12] J. M. Jornet and I. F. Akyildiz, "Channel modeling and capacity analysis for electromagnetic wireless nanonetworks in the terahertz band," *IEEE Transactions on Wireless Communications*, vol. 10, no. 10, pp. 3211–3221, October 2011.

[13] T. Schneider, A. Wiatrek, S. Preussler, M. Grigat, and R. Braun, "Link budget analysis for terahertz fixed wireless links," *IEEE Transactions on Terahertz Science and Technology*, vol. 2, no. 2, pp. 250–256, March 2012.

[14] A. Afsharinejad, A. Davy, B. Jennings, and C. Brennan, "An initial path-loss model within vegetation in the THz band," in *2015 9th European Conference on Antennas and Propagation (EuCAP)*, April 2015, pp. 1–5.

[15] C. Cheng, S. Kim, and A. Zajić, "Comparison of path loss models for indoor 30 GHz, 140 GHz, and 300 GHz channels," in *2017 11th European Conference on Antennas and Propagation (EUCAP)*, March 2017, pp. 716–720.

[16] S. Kim and A. Zaji, "Statistical modeling and simulation of short-range device-to-device communication channels at sub-THz frequencies," *IEEE Transactions on Wireless Communications*, vol. 15, no. 9, pp. 6423–6433, Sep. 2016.

[17] Y. Yang, A. Shutler, and D. Grischkowsky, "Measurement of the transmission of the atmosphere from 0.2 to 2 THz," *Optics express*, vol. 19, no. 9, pp. 8830–8838, 2011.

[18] D. A. Hill, *Electromagnetic fields in cavities: deterministic and statistical theories*. John Wiley & Sons, 2009, vol. 35.

[19] J. F. Johansson and N. D. Whyborn, "The diagonal horn as a sub-millimeter wave antenna," *IEEE Transactions on Microwave Theory and Techniques*, vol. 40, no. 5, pp. 795–800, 1992.